



Pore Structure Characteristics and Gas Storage Potential of the Cretaceous La Luna Formation, Middle Magdalena Valley Basin, Colombia

 Efraín Casadiego-Quintero¹ and  Carlos Alberto Ríos-Reyes²

Received: 03-11-2019 | Accepted: 26-05-2020 | Online: 19-06-2020

doi: 10.17230/ingciencia.16.31.8

Abstract

The rocks of interest in the present study (mudstones) show inherently a heterogeneous pore-size distribution in the matrix. They can present organic and inorganic pores and the transport mechanism through pores is different, and, therefore, it is necessary to describe their organic and inorganic porosity. This work uses different microscopy techniques to characterize mudstones from the Galembo Member of the Cretaceous La Luna Formation, Middle Magdalena Valley Basin, Colombia. These rocks present several pore types, including interparticle pores due to flocculation of clay minerals, organoporosity due to burial and thermal maturity, intraparticle pores from organisms, intraparticle pores within mineral grains, and microchannels and microfractures. The existence of interconnected pores in such complex fracture-pore system provides effective pathways for primary gas migration and it also provides a storage space for the residual hydrocarbon in mudstones, which is important for the primary migration

¹ Universidad Industrial de Santander, ecasageo@gmail.com, Bucaramanga, Colombia

² Universidad Industrial de Santander, carios@uis.edu.co, Bucaramanga, Colombia

and storage in gas reservoir rocks. The pore connectivity is high and increases towards the top of the sedimentary sequence.

Keywords: Gas reservoir; mineralogy; petrography; microstructural; La Luna Formation.

Características de la estructura porosa y potencial de almacenamiento de gas de la Formación La Luna del Cretáceo, Cuenca del Valle Medio del Magdalena, Colombia

Resumen

Las rocas de interés en el presente estudio (lodolitas) muestran inherentemente una distribución heterogénea de tamaño de poro en la matriz. Pueden presentar poros orgánicos e inorgánicos y el mecanismo de transporte a través de los poros es diferente y, por lo tanto, es necesario describir su porosidad orgánica e inorgánica. Este trabajo recurre al uso de diferentes técnicas de microscopía para caracterizar las lodolitas del miembro de Galebo de la Formación La Luna del Cretáceo, Cuenca del Valle Medio del Magdalena, Colombia. Estas rocas presentan varios tipos de poros, incluidos los poros entre partículas debido a la floculación de los minerales arcillosos, la organoporosidad debido a la maduración térmica y el enterramiento, los poros intraparticulares de los organismos, los poros dentro de los granos minerales y los microcanales y microfracturas. La existencia de poros interconectados en este complejo sistema de poro-fractura proporciona vías efectivas para la migración de gas primario y también proporciona un espacio de almacenamiento para el hidrocarburo residual en las lodolitas, lo cual es importante para la migración primaria y el almacenamiento en rocas reservorio de gas. La conectividad de los poros es alta y aumenta hacia la parte superior de la secuencia sedimentaria.

Palabras clave: Reservorio de gas; mineralogía; petrografía; microestructural; Formación La Luna.

1 Introduction

It is well known that worldwide conventional oil and gas supply is declining around the world while costs are going up. In recent years, the energy industry is focusing on the unconventional resources (tight gas sands, coal-bed methane, heavy oil and gas shales), with hydrocarbons in rocks of nano-meter scale porosity and low permeability, now evaluating their potential in many sedimentary basins. Therefore, they are an alternative

promising source of oil and gas supplement. The unconventional gas reservoirs are very important for the petroleum exploration, taking into account that their gas storage properties and potential as a recoverable resource. Gas shales form part of the unconventional gas reservoirs and were considered as viable economic resources after 1970's when United States of America increased the cost of hydrocarbons [1]. They are composed of fine-grained material (clay, quartz, organic matter and other minerals), which can be silty or calcareous and grade into other lithologies. Clay-rich shales are fissile, splitting into thin sheets, although shale types include organic-rich (black) and organic lean (gray or red). Mudstone porosity is 10% and its permeability is very low. Pore spaces between grains are small. Gas occurs in fractures, in pores and adsorbed or dissolved onto organic materials and clays. According to Josh et al. [2], several factors governing whether a particular shale will become a gas shale resource or not, include: (1) organic matter abundance, type and thermal maturity; (2) porosity-permeability relationships and pore size distribution; (3) brittleness and its relationship to mineralogy and rock fabric. Gas shales are generated by (1) primary thermogenic degradation of organic matter; (2) secondary thermogenic cracking of oil and (3) biogenic degradation of organic matter [3],[4]. The evolution of the industry towards new sources of unconventional hydrocarbons has exposed the lack of applicable technology for the characterization of unconventional reservoirs. However, the conventional techniques are not applicable to unconventional reservoirs due to the complex properties of gas shales, and, therefore, while their characterization is very important for production planning, these low permeability rocks are very challenging to characterize due to their complex nano-meter scale pores and mineral structure. Several studies have shown that the results obtained from different analysis can vary significantly. On the other hand, there are some characterization techniques that need to be modified for evaluating mudstones, and many of these issues are addressed in previous studies [4],[5]. Colombia is the third country in South America with the greatest potential for gas shales after Argentina and Brazil. It has 7 high prospectively basins in these resources. However, the focus of interest of this work is the Middle Magdalena Valley basin. Colombia moves forward with 19 exploration processes for potential blocks with unconventional reservoirs. According to reports from the National Hydrocarbon Agency

[6], the country has oil reserves for about seven years, but the focus on unconventional reservoirs hopes to provide new bookings to the country. The potential is approximately 100 million barrels of oil equivalent of which 50% correspond to natural gas. The geological setting of the La Luna Shale play has been the object of several publications and will not be reviewed here [7],[8]. The purpose of this paper is to characterize the variety of pore types that exist in the Galembó Member of the La Luna Formation to evaluate the features that influence gas shale potential and provide a better framework for future economic assessments. The Galembó Member was studied in order to review lateral variations in the hydrocarbon index, because the study area lacks of enough information about the relationship of the geochemical and petrographic characterization of this member. The information generated by this article gives information in which the core data can be correlated with the outcrop data.

2 Geological setting

The Middle Magdalena Valley Basin (MMVB) is a north-south trending intermontane basin located between the Eastern and Central cordilleras of Colombia (Figure 1), which has produced most of the oil and gas in Colombia with over 40 discovered conventional oil fields, sourced out of Tertiary sandstone reservoirs [9]. It has been the focus of shale exploration leasing and drilling activities. Historically, the MMVB has been an important source for the conventional onshore production of hydrocarbons. Several papers about source rocks and petroleum systems have been published [8],[10],[11],[12],[13]. The organic-rich Cretaceous La Luna Formation is the principal source rock in the MMVB. According to Torres [14], the La Luna Formation consists of calcareous black shales and limestones, with high foraminifera content and limestone concretions; based on the facial analysis, the depositional environment is believed to be shallow marine, middle to outer shelf, in a transgressing sea. It has long been considered to be the main hydrocarbon source rock in the MMVB by several authors [10],[12], as well as in other important basins such as the Maracaibo Basin of Venezuela [15],[16] and can be considered as a self-contained source and reservoir system and thus constitutes an unconventional shale play [14].

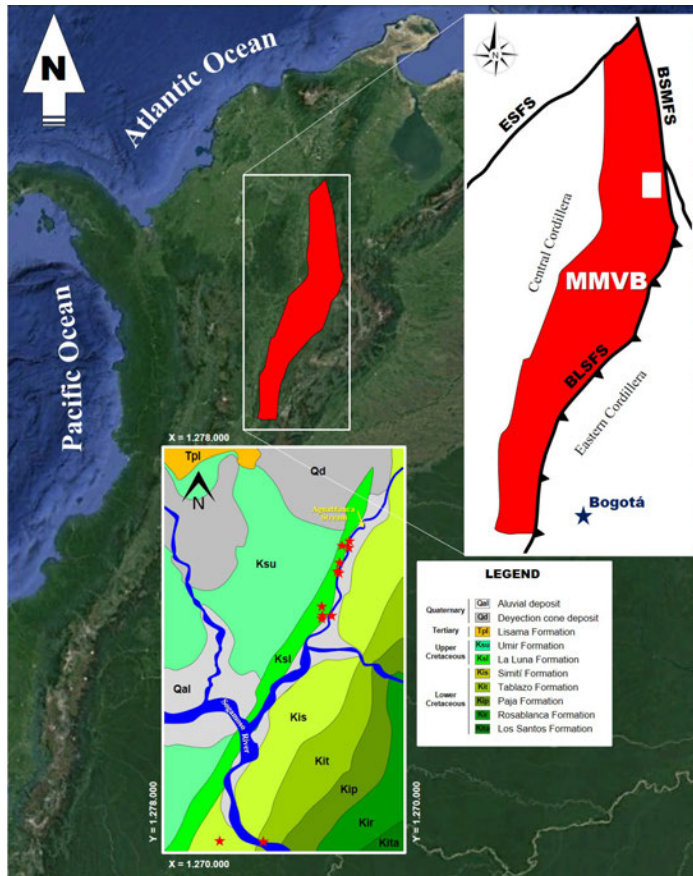


Figure 1: Geographical location of the MMVB (red polygon) in Colombia (adapted and modified from Google Earth [17]), sketch of the MMVB (red polygon) and tectonic limits, showing the study area (adapted and modified from ANH [6]), and generalized geological map showing the sampling localities. BLSFS, the Bituima - La Salina Fault System; ESFS, the Espiritu Santo Fault System; BSMFS, the Bucaramanga - Santa Marta Fault System.

The La Luna Formation in the MMVB is similar to the one described in Venezuela [10]. However, in the MMVB, previous workers [7],[12]; have divided it into three members from base to top: Salada (hard, black, thinly bedded, finely laminated, limy shales with some thin beds of black fine-grained limestones; abundant planktonic foraminifera and radiolarian but

lacks benthonic foraminifera), Pujamana (gray to black, calcareous, thin bedded shale) and Galembo (thinly bedded, black, calcareous shale with interbeds of thin argillaceous limestones; thin beds of blue-black cherts and numerous ammonite bearing concretions occur). The three members of the La Luna Formation contain variable carbonate contents: The Galembo Member generally contains minor-to-trace amounts of carbonate (2.4%), in contrast, the Pujamana and Salada members are carbonate-rich (43.2% and 40.4%, respectively) [10]. The thickness of the Galembo Member can range from 180 to 350 m [7] to the north of the Middle Magdalena Valley Basin. According to Piamonte & Mayorga [18], who raised a stratigraphic column in the Quebrada La Sorda Section, 10 km north of the study area of this work, the thickness of the Galembo Member ranges from 186 to 200 m. Total Organic carbon (TOC) values in the Pujamana and Salada members average approximately 3.5 wt% and 4.5 wt%, respectively [10], whereas TOC values in the Galembo Member reach 2.4% [12].

3 Field sampling and analytical methods

The investigated samples come from the Galembo Member of the Cretaceous La Luna Formation, which were collected from several relatively fresh outcrops along the eastern flank of the Nuevo Mundo Syncline in the MMVB approximately 20 km west of Bucaramanga, Colombia. A stratigraphic column of about 50 m of thickness was described in the section of the Aguablanca Stream. It was accompanied by a systematic sampling. The classification of Folk [19] for terrigenous rocks and Dunham [20] for allochemical/orthochemical rocks were adopted in the classification. Mineralogy analysis performed by collecting X-ray powder diffraction (XRPD) patterns. Samples were milled in an agate mortar and then mounted on a sample holder of polymethylmethacrylate (PMMA) by the technique of filling front. The XRPD pattern of garnet was recorded by X-ray diffraction using a BRUKER D8 ADVANCE diffractometer operating in Da Vinci geometry and equipped with an X-ray tube ($Cu - K\alpha_1$ radiation: $\lambda = 1.5406 \text{ \AA}$, 40 kV and 30 mA), a 1-dimensional LynxEye detector (with aperture angle of 2.93°), a divergent slit of 0.6 mm, two soller axials (primary and secondary) of 2.5° and a nickel filter. Data collection was carried out in the 2θ range of 12-80, with a step size of $0.01526^\circ(2\theta)$ and counting time

of 1 s/step. Phase identification was performed using the crystallographic database Powder Diffraction File (PDF-2) from the International Centre for Diffraction Data (ICDD) and the program Crystallographica Search-Match. The unit-cell constants, atomic positions, factors of peak broadening and phase concentrations were refined and calculated by using the MDI RIQAS program based on Rietveld method. 29 thin sections were prepared for petrographic analyses from offcuts of the rock samples with the plane of the section normal to the macroscopic lamination. All samples were impregnated with epoxic resin and stained for carbonates and feldspars and also to recognize the porosity. Thin sections were point counted (300 grains per sample) using the Gazzi-Dickinson method [21]. Petrographic analysis was performed using a trinocular Nikon (Labophot2-POL) transmitted light microscope equipped with an Olympus DP71 camera for image acquisition. Mineral abbreviations are after Kretz [22]. More detailed analyses followed by means of environmental scanning electron microscopy (ESEM) using a FEI QUANTA FEG 650 instrument, under the following analytical conditions: magnification = 800-60000x, WD = 5.6-14.0 mm, HV = 10.0-20.0 kV, signal = ETD/Z CONT, detector = SE/BSED. Operational mode was mainly using secondary electrons (SE), although back scattered electrons (BSE), were also useful where contrasts in grey level in the images correspond to contrasts in atomic number and therefore chemical composition of the analyzed area. Particular areas of interest were analyzed to retrieve the chemical composition of the region via energy dispersive X-ray spectroscopy (EDS). EDS Detector EDAX APOLO X with resolution of 126.1 eV (in. Mn $K\alpha$).

4 Results and discussion

4.1 Lithofacies

The Galembo Member of the La Luna Formation comprises a variety of lithofacies, which, with the exception of volcanic ash falls, are dominated by fine-grained (clay- to silt-size) sediments. Casadiego [23] recognized five lithofacies in the Aguablanca section (Figure 2) on the basis of mineralogy, fabric, fossil content and texture: (1) nonlaminated to slightly laminated foraminifera wackestones, (2) highly fossiliferous moderate- to

well-laminated organic-rich mudstones; (3) claystones with fossiliferous carbonate concretions with pyrite; (4) nonlaminated siliceous and fossiliferous claystones; (5) volcanic ash falls. These lithofacies will be discussed briefly in the sections below. The Galembo Member facies were defined from descriptions of outcrops in the Aguablanca section. Collectively, the analyzed outcrops show that the upper and lower part of the Galembo Member are composed dominantly of nonlaminated and slightly laminated foraminifera wackestones, highly fossiliferous moderate- to well-laminated organic-rich mudstones (sometimes with fossiliferous carbonate concretions with pyrite), and nonlaminated siliceous and fossiliferous claystones, with interlayered thin layers of volcanic ash falls.

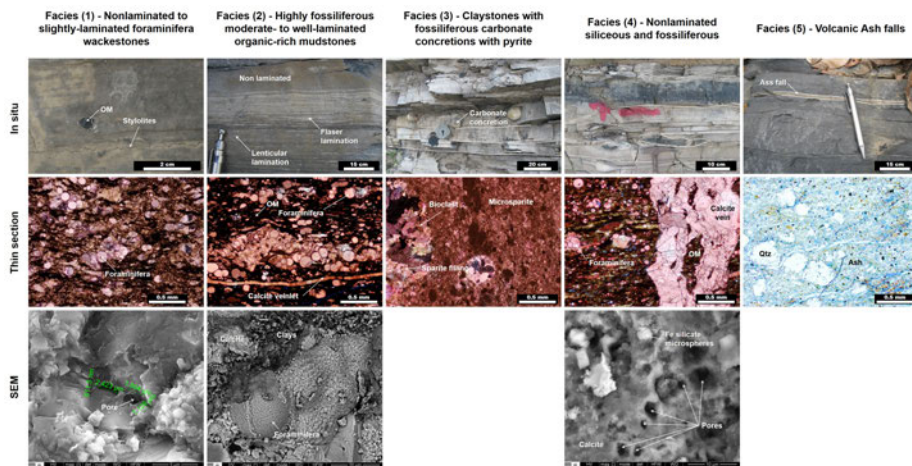


Figure 2: Photographs showing outcrops of the Galembo Member of the La Luna Formation in the Aguablanca section and representation of their features seen in petrographic section and SEM micrographs.

4.1.1 Nonlaminated to slightly-laminated foraminifera

wackestones. This lithofacies represents the 35% of the Galembo Member interval in the Aguablanca section, although these rocks are highly variable in character. Vertical changes from one lithofacies to another can be sharp or gradational. Nonlaminated to slightly-laminated foraminifera wackestones show irregular contact with highly fossiliferous moderate- to well-laminated organic-rich mudstones and contains intercalations of clay-

stones with fossiliferous carbonate concretions with pyrite and volcanic ash falls. Fabric ranges from nonlaminated to slightly laminated. Non-laminated rocks are not affected by bioturbation. These rocks are mainly medium dark gray in color, although thin layers with higher content of fossils display light gray color. On the other hand, fragments of white broken shells obliquely arranged are embedded in the matrix. Stylolites and agglomerates of organic matter were observed.

4.1.2 Highly fossiliferous moderate- to well-laminated organic-rich mudstones. This lithofacies is the predominant lithofacies in the Aguablanca section (64%). This lithofacies is interlayered with foraminifera wackestones to the base and siliceous and fossiliferous claystones to the top. Its average layer thickness (0.3 to 4 m) tends to increase towards the top of the section. Most of all contacts with overlying and underlying siliceous and fossiliferous claystones are straight and sharp. Fabric ranges from nonlaminated to slightly laminated to the bottom and lenticular to flaser laminated and laminar to massive structure towards the top. These rocks display a dark to middle gray color.

4.1.3 Claystones with fossiliferous carbonate concretions with pyrite. This lithofacies constitutes 5% of the Aguablanca section. It is characterized by the occurrence of fossiliferous concretions with pyrite, with numerous subrounded very light gray to medium light gray carbonate concretions up to 30 cm in thickness formed in a state of early diagenesis due to early burial. Most concretions contain fossils such as bivalves and ammonites and pyrite. These rocks also include dark grey claystones interlayered with fossiliferous organic-rich claystones. Claystones with fossiliferous carbonate concretions with pyrite show irregular contact with the underlying and overlying layers, although they show a well-defined contact with highly fossiliferous moderate- to well-laminated organic-rich mudstones. Fabric is laminated. It consists entirely of microsparite and recrystallized microsparite. Within concretions fragments of bioclasts filled with sparite were observed. It shows a predominantly calcareous composition, with a few crystals of pyrite and organic matter.

4.1.4 Nonlaminated siliceous and fossiliferous claystones. This lithofacies represents the 1-5% of the Aguablanca section and is characterized by the appearance of microcrystalline silica, moderate content of foraminifera and massive sedimentary structure. Reaction with acid is very low. These rocks show a grayish black to dark gray color, developing layers up to 15 cm in thickness, and are scarcely distributed mainly at the top of the section, particularly interlayered into highly fossiliferous moderate- to well-laminated organic-rich mudstones, developing irregular and well-defined contacts.

4.1.5 Volcanic Ash falls. They represent the least common lithofacies in the Aguablanca section (1%), which occurs as very thin layers (up to 2 cm in thickness) in the base, which are rich in kaolinite and silica. It displays a pale yellowish-orange color with flecks of very pale orange color that can be attributed to the strong weathering. They are in well-defined contact with highly fossiliferous moderate- to well-laminated organic-rich mudstones. This lithofacies shows a long extension and lateral continuity despite its thickness, low hardness compared to the underlying and overlying layers, and easy disintegration. In some layers on the top, it shows higher silica content whereas in the underlying claystones ripple marks or disturbance of the lamination due to variations of energy during deposition can be observed. It shows a well-defined contact with the underlying claystone layers and gradual transition with the overlying layers. It consists of microcrystalline quartz of tabular habit. The volcanic ash falls can be zeolitic tuffs, produced by volcanic eruptions, which expelled very fine-grained volcanic ash that were airborne, later falling on marine waters and deposited on the bottom.

4.2 Mineralogy and lithology

Thin-section, scanning electron microscopy and X-ray diffraction analysis reveal that the Galembo Member rocks generally contain less than one-third clay minerals, which are dominantly illite with minor smectite. Silica (clay- to silt-size crystalline quartz) is by far the dominant mineral; carbonate (clay- to silt-size crystalline calcite and dolomite) is also locally common, along with lesser amounts of pyrite and phosphate (apatite). Carbonate is

mostly in the form of fossils. This calcite-dominated skeletal debris is locally common throughout the section. A detailed analysis of the Galembo Member mineralogy was performed by Casadiego [23]. A ternary diagram of their mineralogical constituents show that the analyzed samples are composed mainly of allochemical, orthochemical and terrigenous minerals in different proportions with abundant proportions of carbonate planktonic foraminifera species and other pelagic organisms, suggesting deposition in moderately deep water with restricted bottom circulation. The rocks of the Galembo Member are within the range of mudstones. The mineral composition was determined under the transmitted light microscope, which was compared with data from X-ray diffraction. The carbonate material is mainly rhombohedral dolomite, micrite, foraminifera, calcareous sponge spicules, bioclastic limestones and calcareous cement. The siliceous material includes sponge spicules, bioclasts filled with microcrystalline silica and chert, quartz and chert grains, siliceous matrix and cement. Other accessory minerals (feldspar, pyrite, zircon, opaque minerals and phosphates) comprising less than 3% of the rock were observed.

4.3 Grain size and fossil content

The different grain sizes found in the Aguablanca section correspond to carbonate and siliceous bioclasts, grains of quartz and intraclasts. Planktonic foraminifera species are very common and abundant (15-40%), with minor amount of bivalve shells and undifferentiated bioclasts (8-10%), and scarce amount of echinoderms (<5%). The fragments of calcareous fossils are seen mainly in nonlaminated to slightly laminated foraminifera wackestones and in minor amounts in highly fossiliferous moderate- to well-laminated organic-rich mudstones and nonlaminated siliceous and fossiliferous claystones. Fossil fragments sometimes display replacement with chert and phosphate were observed in relative low abundance toward the upper-middle part of the Aguablanca section. Silt-sized quartz grains of sub-angular to subrounded shape occur in trace amounts (<1%); they are not observed in laminations and use to appear as floating grains isolated in the clay matrix of volcanic ash falls. Clay or organic matter intraclasts are present in traces (<3%), mainly towards the bottom of the section. The interclasts are dark- to light-gray silt-sized granules, showing evidence of

compaction. Compositional and textural features of siliceous and fossiliferous claystones are shown in Figures 3 and 4.

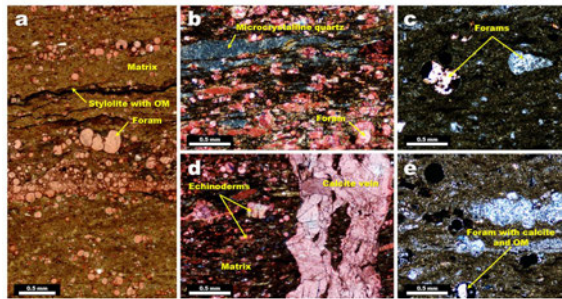


Figure 3: Compositional and textural features of siliceous and fossiliferous claystones: (a) siliceous argillite with parallel stylolites OM fillings anastomosing type, (b) microcrystalline quartz lenses, (c) and (e) planktonic foraminifera filled with microcrystalline quartz and calcite with OM, (d) morphology matrix in SEM, (e) filled microfractures calcium carbonate (pseudosparite and sparite).

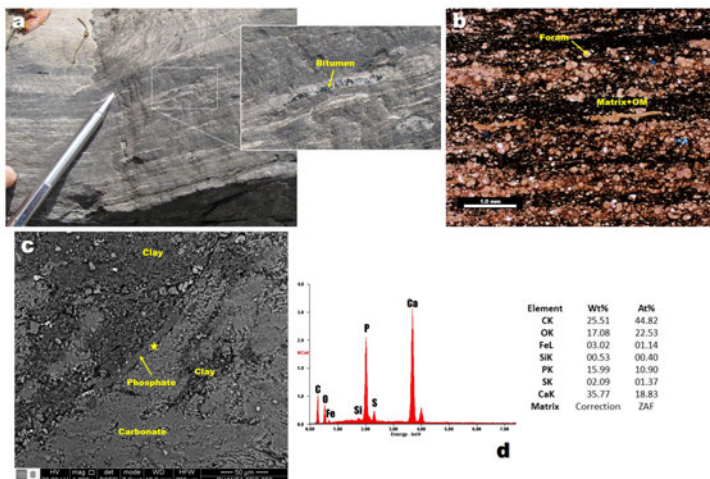


Figure 4: Compositional and textural features of highly fossiliferous claystones rich in organic matter: yellow star indicating EDS of phosphate. Organic matter was observed between laminated foraminifera. EDS, Energy Dispersive Spectroscopy. OM, Organic Matter.

The occurrence of pyrite and organic matter is predominantly toward the top of the section, where the last of them is observed by filling fractures, bioclasts and forams (Figure 5a). Compaction increases as clay mineralogy increases (Figure 5b). Dissolution of forams previously filled with carbonate (Figure 5c) was observed. Deformation generated in the claystones with fossiliferous carbonate concretions with pyrite is attributed to the early diagenesis, which as concretions formed, adjacent layers beginning to deform. Lamination by interlayered forams and clays reveal this deformation. Mud to fine-grained sandy particles are mainly planktonic foraminifera species (*Globigineroides* and *Globigirined*), with traces of benthonic foraminifera (*Textularia*), echinoderm spicules, fish bones and fragments of broken gastropods (Figure 6) possibly transported by submarines flows of low density.

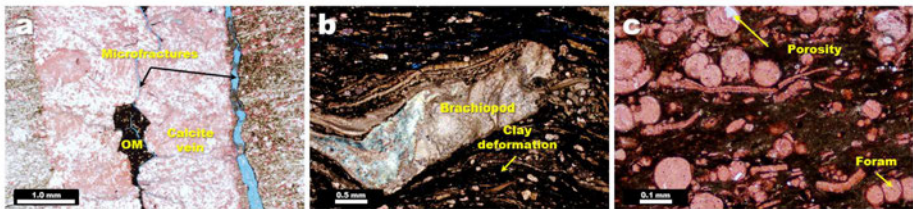


Figure 5: Microphotographs of (a) fractured filled with calcite, which is also filled with organic matter OM); (b) deformation of clay matrix; (c) moldic porosity of forams due to carbonate dissolution.

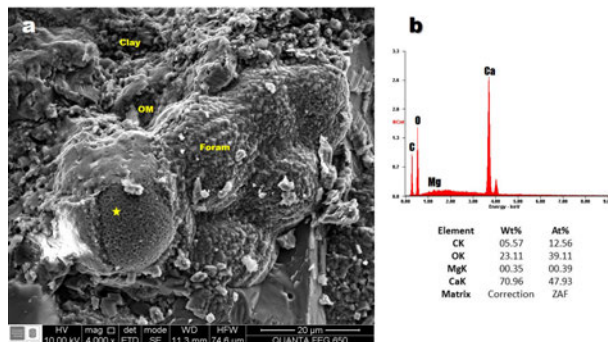


Figure 6: Globigerina shell replacement with calcite. Yellow star indicates the analytical point where the EDS was obtained. EDS, Energy Dispersive Spectroscopy.

4.4 Fabric

FEG ESEM analysis allowed recognizing the fabric of the analyzed samples at a microscopic scale, providing valuable data on the clay morphology, occurrence of fossils and organic matter, and micro and nano-meter scale porosity, and the pattern of distribution of clays. The observed association between clay particles was primarily face-to-face configured as multi-imbricated and edge-to-face [24]. Mudstones are characterized by poor bioturbation, which helps to preserve the original depositional rock texture. FEG ESEM images of Figure 7 illustrate how clays (mainly of illite type) were deposited, with clay particles deposited in a dispersed form on the lower part of the section, possibly in a deep water column, and clay particles with a floccular domain structure (clay particles are grouped each other by edges) in the upper part of the section, probably associated to a water column less dense than the underlying clays which allowed to keep the initial orientation in which they were deposited [24],[25]. The content of organic matter in the analyzed samples depends on the bulk rock chemistry alternating with changes in the microstructure and grain size (mainly foraminifera and clay-sized minerals) that generate laminations [25], which are rhythmic repetitions due to energy variation of sea floor currents influencing the production or transportation of floccules (Figure 8a). According to the generated energy, there is a selection of the foraminifera size, as well as an orientation of clays (Figure 8b) and foraminifera (Figure 8c). According to Casadiego [23], results from TOC, XRD and SEM reveal that samples with higher content of clay minerals have more content and better preservation of organic matter, which can be interrupted with the deposition of silt-sized grains and abundant content of calcareous mineralogy. In general, higher marine organic content is associated with more fine-grain lithofacies (e.g., mudstones), in rocks with very high TOC content (e.g., > 5 wt% TOC), there is negative correlation of clay mineral wt% and TOC wt%, which can be explained as a result of the dissolution of the TOC due to detrital material (often clay-size particles) [4]. This is described in detail in previous studies [4],[26].

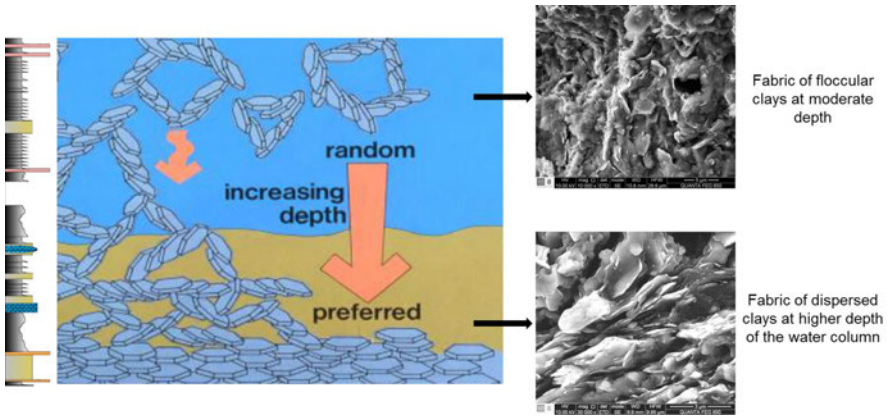


Figure 7: Fabric from dispersed (bottom) to floccular (top) clays of the Galembó Member of the La Luna Formation in the Aguablanca section (adapted and modified after O'Brien & Slatt [25]).

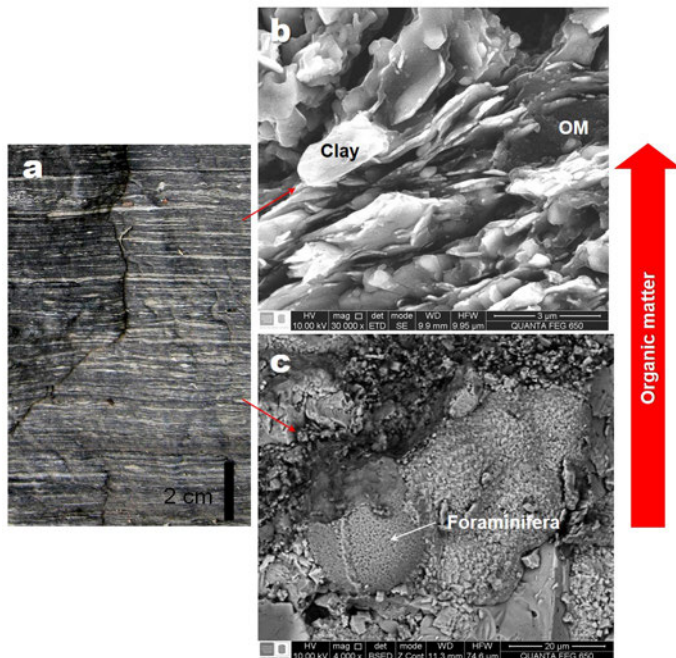


Figure 8: Variation of organic matter with lamination. OM, organic matter.

4.5 Pore microstructures

Conventional rock typing methods use petrographic observations, including image analysis to determine pore types qualitatively or quantitatively in an attempt to relate the pore system, at least in part, to flow and textural pore types [27]. However, such methods do not resolve the complexity of the pore system in mudstone rocks. In a total porosity system, all intergranular and intragranular porosity potentially could host hydrocarbons. However, previous studies of clay-rich organic-rich mudstones [4] have shown that in some shale-gas reservoirs, essentially all of the inorganic porosity (e.g., between the clay grains) is full of irreducible capillary-bound water, so when $\text{TOC} \ll 1 \text{ wt\%}$, the rock is mostly full of water; when there is TOC present, the total porosity of the rock doubles (from 8% to about 16%), but measurements of S_w indicate that the amount of water remains the same, suggesting that the gas is occupying 8% organic porosity, in addition to the 8% porosity filled with capillary bound water. Therefore, just because there is pore space, doesn't mean that that hydrocarbons will actually reside in that pore space. The nice thing about shale-gas reservoirs, is that the pores within organic matter are filled with gas (both free gas and adsorbed gas on the surface of hydrocarbon-wet organic pores) [4]. Recent developments of advanced microscopy allow study of pore microstructures of shales by scanning electron microscopy - SEM [28],[29],[30],[31],[32], focused-ion-beam and scanning electron microscopy - FIB SEM [33],[34], broad-ion-beam and scanning electron microscopy - BIB SEM [35],[36]. These technologies have emerged as very powerful tools for characterizing pore microstructures; however, appropriate sample preparation is critical to obtain high-resolution images with minimal artifacts. In the following sub-sections, observations are only based on FEG-ESEM images of fractured surfaces, which allow investigating not only the topography and the nature and arrangement of mineral phases but also the pore microstructures of the Galembó Member shales at the Aguablanca section as shown in Figure 9. According to Loucks et al. [37], the pores within gas shales can be grouped into three types: (1) mineral matrix pores between or within mineral particles; (2) pores within organic matter and (3) fracture pores that are not controlled by individual particles.

We adopt the classification proposed by Slatt & O'Brien [29] to describe the pore types that are present in the Galembo Member of the La Luna Formation. FEG-ESEM analysis reveals that analyzed samples show an important porosity, with some differences in the recognized lithofacies. Porosity may be expressed in several types (Figure 10), which are described in detail below.

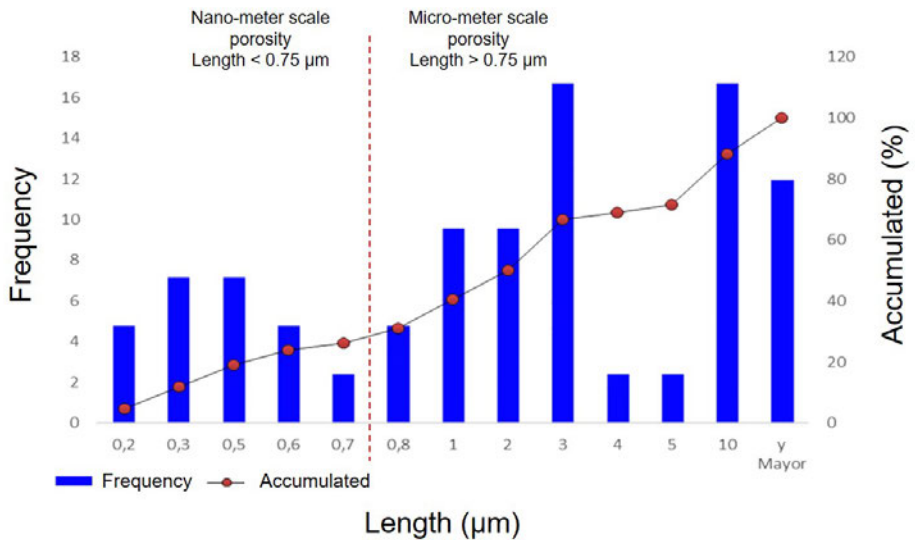
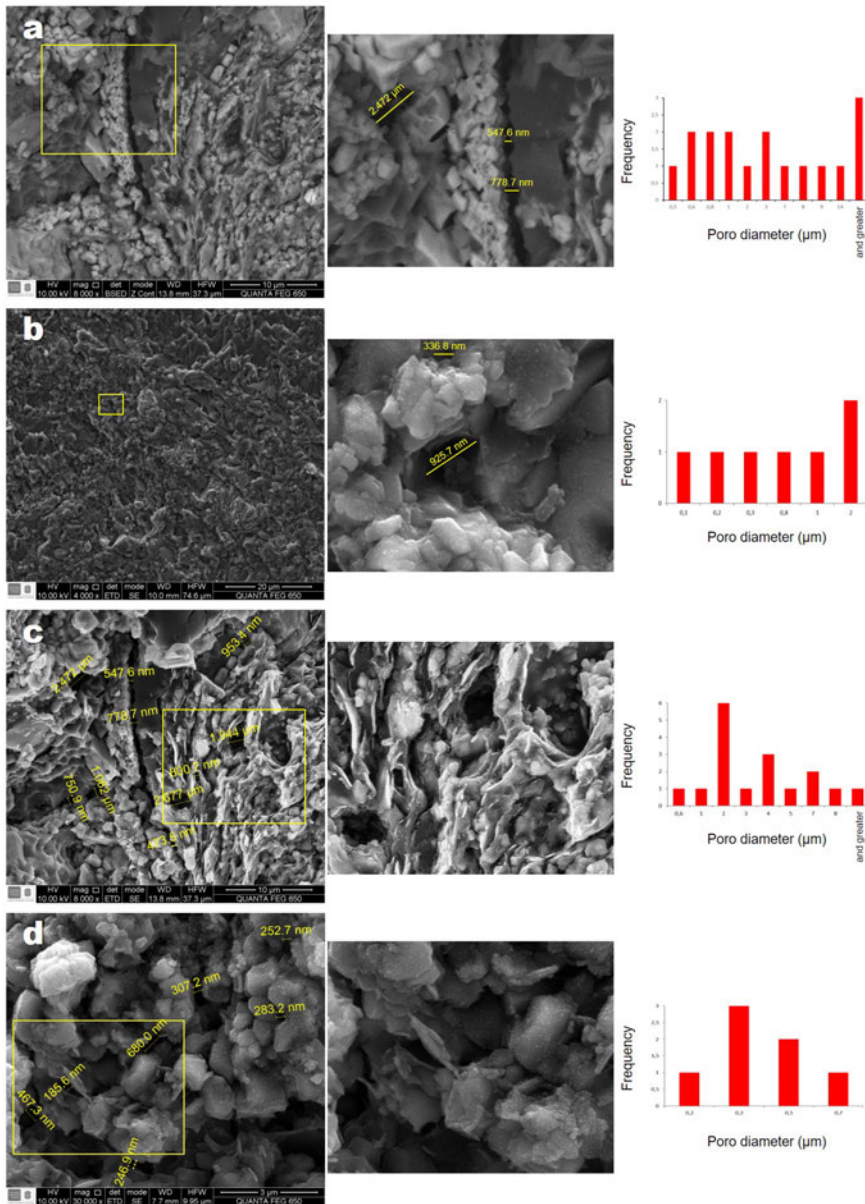


Figure 9: Variation of porosity in samples of the Aguablanca section analyzed by FEG ESEM. Red dashed line is the limit proposed by Slatt et al. [32] to differentiate nano-meter scale porosity and micro-meter scale porosity.



4.5.1 Interparticle pores due to flocculation of clay minerals.

Particles of clay minerals (illite) are mainly present in highly fossiliferous moderate- to well-laminated organic-rich mudstones. The interparticle pores commonly have an irregular morphology and are larger than organic matter pores. They occur typically at grain contacts and filling the intergranular volume, with non-clay minerals, such as quartz and calcite systematically coated with illite, which use to develop cleavage pores, although interparticle pores are elongated parallel to the adjacent surface of non-clay minerals.

In general, they form layers of open nano-meter to micro-meter scale flakes (Figures 11a-c). However, they also use to develop clay floccules (Figures 11a-b), which can form a "cardhouse" structure of individual edge-face- or edge-edge-oriented flakes similar to what is reported by other authors [24],[25],[29], which may form pores of 0.2-0.7 μm .

According to Slatt and O'Brien [29], this cardhouse pattern provides pores between the floccules that are larger than the 0.38-nm diameter of methane molecules. These pores are sometimes interconnected, developing permeability pathways for gas fluid as suggested by Slatt et al. [32]. The connectivity of this type of pores is high and increases towards the top of the Aguablanca section. However, according to Slatt & O'Brien [29], it is not clear how clay floccules dominating the microstratification of such rocks could have survived burial and diagenesis for up to hundreds of millions of years. Clay minerals sometimes show dissolution at the edges likely due to a post-deposition process during early diagenesis. If this process continues, the porosity may increase.

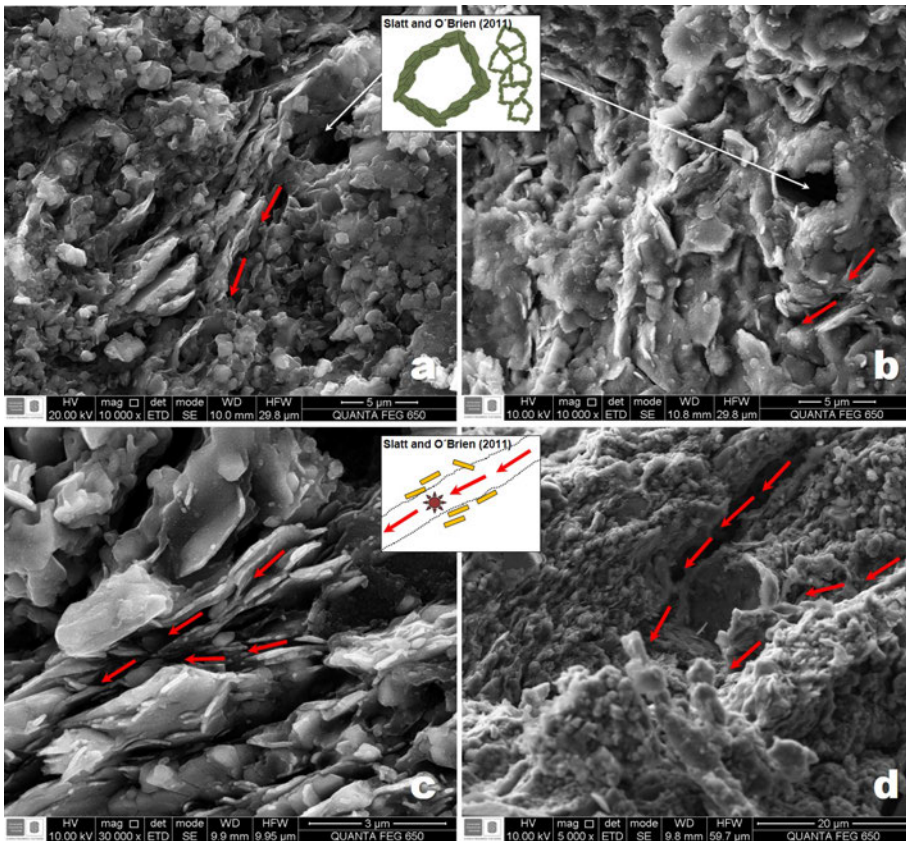


Figure 11: Interparticle pores due to flocculation and microchannels developed in clayed lithofacies.

4.5.2 Organoporosity due to burial and maturation. . This type was first reported by Loucks et al. [35], and according to Jarvie et al. [38], these pores are generated during burial and maturation of organic matter. We also report the occurrence of organoporosity in nonlaminated to slightly laminated foraminifera wackestones in two ways: (1) organic matter with a pendular morphology filling pore spaces between calcite crystals, with pores showing an elongated and angular shape, some of them interconnected; (2) laminar solid organic matter with low content of interconnected microporous space, with isolated pores, which according to Loucks

et al. [37] can be associated to immature organic matter. The pendular morphology observed is likely partially drained organic matter filled intragranular pores, and not true Passey et al. [4], this drained feature can occur throughout the oil-window, but the nano-meter scale organic pores typically are present from $R_o = 0.8$ through the entire gas window ($R_o > 3$), and the fact that He-porosimetry gives porosity values much higher than Mercury Injection Capillary Pressure porosity, indicates that much/most of the nano-meter scale organic pores are connected, but that the pore throat size is < 3 nm - well below the resolution of even Broad Ion Beam or Focus Ion Beam Scanning Electron Microscopy. This ultratiny porosity has been successfully imaged using Scanning Transmission Electron Microscopy [5].

4.5.3 Intraparticle pores from organisms. Organisms may produce intraparticle porosity by bioturbation of sediments, by generation of fecal pellets, and by the porous nature of their skeletons or shells [29]. The Galembó Member shales contain abundant fossil content, including planktonic (*Globigineroides* and *Globigirined*) and benthonic (*Textularia*) foraminifera species, spicules of echinoderms, broken gastropods and bivalves, and fish bones.

4.5.4 Intraparticle pores within mineral grains. The Galembó Member shales are characterized by the occurrence of occasional pyrite framboids, which are composed of several small pyrite crystals between which a small number of intraparticle pores from 0.2 to 0.3 μm occur as shown in Figures 12a-b. Organic matter is sometimes observed associated to pyrite framboids, which is indicative of anaerobic diagenesis sulfides [32]. Quartz grains and flakes of clay minerals oriented around pyrite framboids develop micropores of 2-4 μm (Figure 12b). Other pores are also observed in fossil fragments (Figures 12c-d). In the lithofacies dominated by calcareous clays, calcite in micrite ranges from 0.8 to 3 μm and contains intraparticle pores. Sparite mainly occurs as cement in nonlaminated to slightly laminated foraminifera wackestones. It is characterized by crystals ranging in size from 1 to 3 μm , poor preservation of shape, and moderate dissolution, which is a process that can be attributed to crystallization at a late stage of diagenesis [39]. The pores are in the range 0.1-2 μm . The pore connectivity is low, but it increases with the preservation of foraminifera that have not

undergone dissolution. Pores in siliceous matrix are mainly observed in the siliceous lithofacies, which can be attributed to as the result of the mixture of clay minerals and volcanic ash flows on the sea floor, the high content of iron (hematite) and silica as cement, and the presence of planktonic foraminifera species, which show replacement with microcrystalline quartz. Intraparticle porosity is not clearly observed, because pores are cemented by silica, showing very poor connectivity. A vesicular texture due to rapid cooling of volcanic ash is observed.

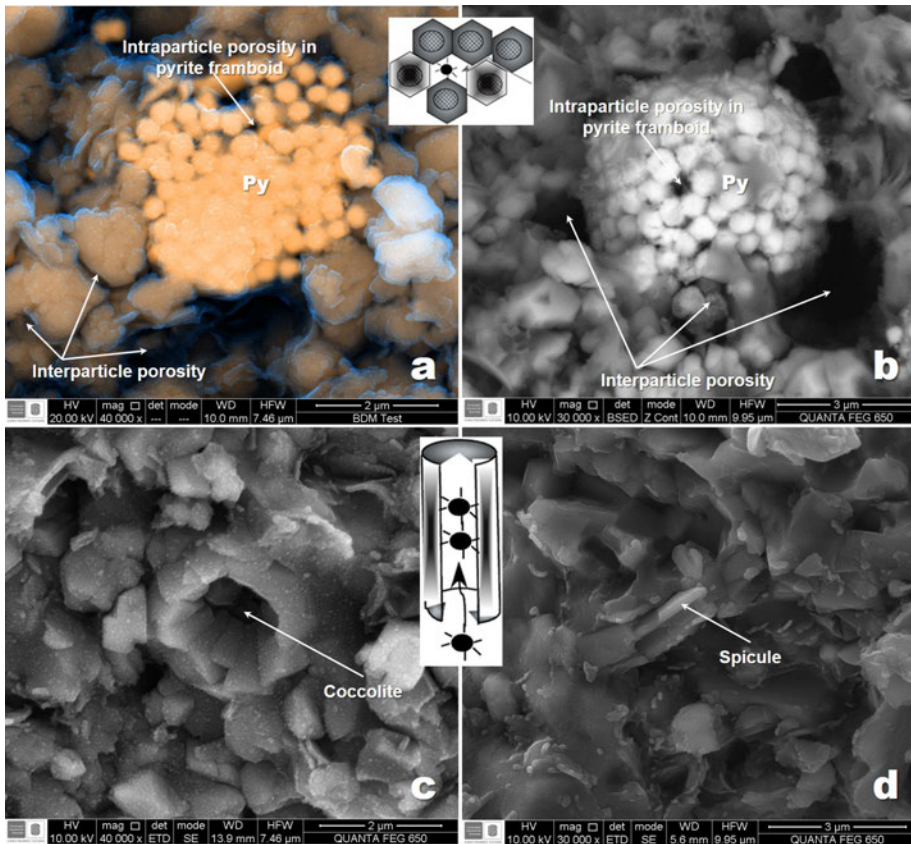


Figure 12: Intraparticle pores associated to (a)-(b) pyrite framboids and (c)-(d) fossil fragments.

4.5.5 Microchannels and microfractures. The Galembó Member shales shows several examples of microchannels (elongate pores), which occur within the matrix of shale (Figure 13).

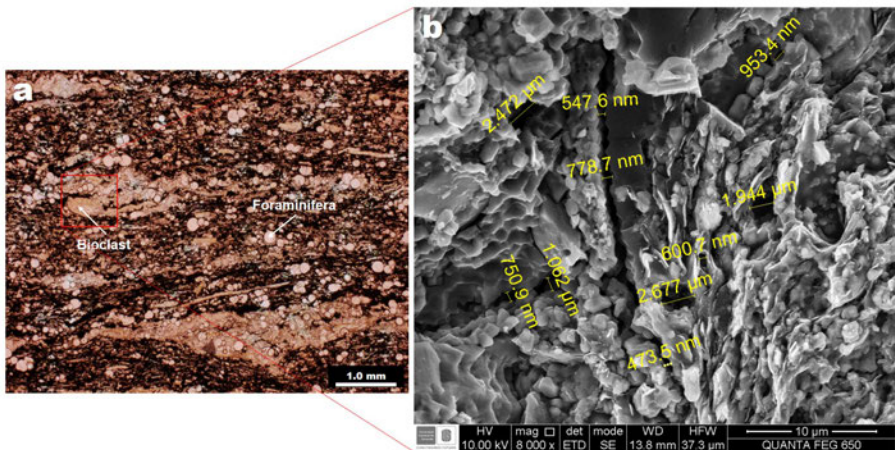


Figure 13: PPL photomicrograph (left) and SEM image (right) of the microporosity between clayed calcareous mud and rigid bioclasts. PPL, plane polarized light; SEM, scanning electron microscopy.

Microchannels are of millimeter scale in width, which is wide enough to provide a permeability passage for gas flow. However, how much of these millimeter scale channels are part of the original rock texture, taking into account that these are likely the result of mechanical behavior of the rock? On the other hand, microchannel also occur at the boundary between rigid bioclasts (mainly foraminifera displaying replacement with calcite, gastropods and bivalves) and shale matrix. They may be filled with organic matter, with horizontal fractures filled with organic matter (depositional). These microchannels, if abundant, they could provide significant permeability hydrocarbon migration pathways, in addition to microporosity [29]. They show a sinuous and discontinuous shape and are following the stratification plane. According to Slatt & O'Brien [29], microchannels cannot be interpreted as artifacts produced by pressure release when fracturing the sample during handling and preparation, but represent original microchannel openings preserved in the undisturbed shale matrix. Slatt et

al. [32] concluded that they are not parting planes parallel to bedding based on the following observations: (1) microchannels do not extend across the entire viewing area of the sample on a SEM stub nor at the core plug scale; (2) they are not perfectly horizontal and parallel to bedding; and (3) they form stair-step pattern. Microfractures in shales occur at a variety of scales [32],[40] and are significant in any fabric investigation of shale properties, particularly those related to artificial fracture treatment [29].

In the Galembó Member shales, natural microfractures are usually related to vertical fractures filled with calcite veins, which may be also filled with organic matter or partially open. Nonlaminated to slightly laminated foraminifera wackestones shows few microfractures occupy 1% of the rock volume, with calcite filling 80-96% of these fractures and 14-20% of them still open or filled with some other non-calcite material. The porosity is mainly associated to foraminifera dissolution. Highly fossiliferous moderate- to well-laminated organic-rich mudstones present a porosity of 3% due to microfractures filled with organic matter, which was also later filled with pseudosparite and sparite (Figure 14) and foraminifera dissolution (Figure 15).

Most of these microfractures are perpendicular to lamination and their opening are of millimetric and micrometric scale [32],[39]. In the contact between the sparite veins and clay minerals, planes of weakness that induce new fractures which can be formed at the time of sampling or when changing the pressure conditions of the rock [40]. Nonlaminated siliceous and fossiliferous claystones show microfractures with openings from 0.6 to greater than 8 μm , which sometimes display a sinuous shape in some smooth walled straight intervals, and may be interconnected.

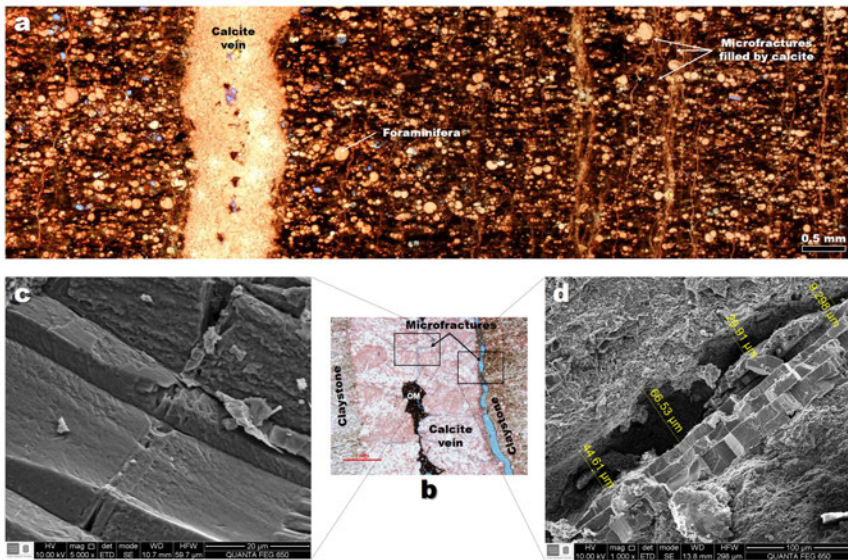


Figure 14: (a) Microfractures perpendicular to lamination. Note the calcite-filled fracture, which was then filled with organic matter, and the microfractures within the calcite vein and in the contact between the main fracture and clay minerals. (b) XPL photomicrograph of calcite-filled fracture, which was then filled with organic matter. (c)-(d) SEM images of the occurrence of microfractures and fillings. XPL, cross-polarized light; SEM, scanning electron microscopy.

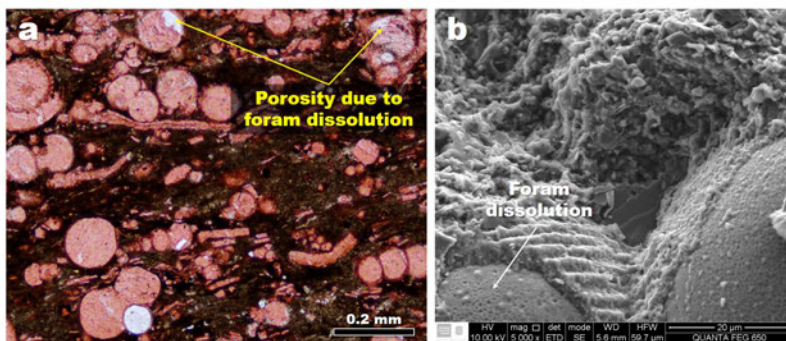


Figure 15: XPL photomicrograph (left) and SEM images (right) of the foraminifera porosity due to carbonate dissolution. XPL, cross polarized light; SEM, scanning electron microscopy.

We illustrate several examples of a variety of pore types that are present in the Galembo Member of the La Luna Formation, using the classification proposed by Slatt & O'Brien [29]. The pores observed in the analyzed samples are sufficient not only to store hydrocarbon molecules but also to promote their flow through pathways. Porosity is associated to flocculation of clays probably with greatest potential, along with microfractures and organoporosity, to provide storage places as well as permeability pathways for migration of hydrocarbons. The storage and migration of hydrocarbon molecules through mudstones is complex, slow and not fully understood, owing to the small pore size and capillary properties, and, it is for this reason that almost all shales require artificial fracturing to obtain commercial flow rates [41].

The porosity resulting from depositional and diagenetic processes are influenced by several factors, such as compaction, cementation and dissolution of minerals. Claystones can show greater compaction and deformation, where it is possible to distinguish the deformation around bioclasts and discontinuous laminations of organic matter. Samples with high content of carbonate and phosphate exhibit little compaction and moldic porosity (3%). Samples with high content of pyrite and quartz do not show dissolution and show very low compaction. Samples with the highest quartz content (> 40%) often exhibit microfractures perpendicular to lamination, which are filled with organic matter (likely bitumen) or carbonates (Figure 16).

A generalized sequence of diagenesis observed in the Galembo Member rocks is summarized in Figure 17.

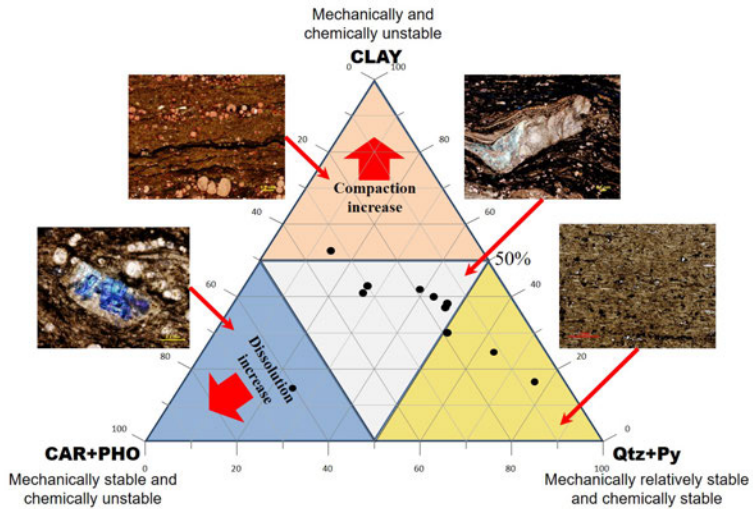


Figure 16: Compositional diagram showing the claystones that show relationship stability between mineralogy, fabric, texture, organic matter and porosity.

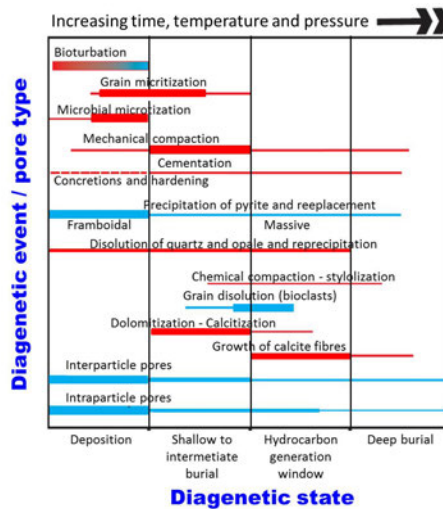


Figure 17: Generalized sequence of diagenesis of the muddy rocks burial. Bars in blue and red are contributions to the porosity and cementation, respectively (modified after Loucks et al. [37]).

4.6 Brittleness Index

According to Slatt et al. [32], common characteristics of shales influence their geomechanical properties (ductility and brittleness) depending on the state of rock deformation, which can be recognized at different scale. Ductile rocks are more likely to deform in response to stress before breaking, which is characteristic of clay- and organic matter-rich mudstones. On the other hand, brittle rocks are highly elastic and have low ductility, fracturing easily, which is typical in rocks with higher content of calcite and quartz. The brittleness index is a function of the mineral composition, diagenesis and organic content [38]. Brittleness index is one of the critical geomechanical properties for shale reservoir rocks to screen effective hydraulic fracturing candidates [42]. According to Lou et al. [43], it can be influenced by mineral composition and particle size distribution. The brittleness index was calculated for the Galembó Member using Equation (1) proposed by Wang & Gale [44], which is assumed by the ratio of the phases as quartz, calcite and dolomite that tend to increase the brittleness on phases, such as clays and organic matter, and other phases detected by X-ray diffraction, that tend to increase the ductility [45]. Rocks with large numerical values of Poisson's ratio and low values of Young's modulus have a lower brittleness index, therefore, they are ductile, while rocks with a Low Poisson ratio and a large Young's modulus have a higher brittleness index and are known to be brittle [46],[47]. In theory, when comparing the geomechanical data of the Young and Poisson module with the fragility index obtained from the composition, the rock behavior is similar in both methods.

$$BI = \frac{(quartz + calcite + dolomite)}{(quartz + calcite + dolomite + clay + OM)} \quad (1)$$

where BI is the brittleness index and OM is organic matter. We use the data obtained for S2 regarding the content of organic matter, which according to previous studies [14],[48] follow a similar trend to TOC. The average value from higher to lower brittleness of the lithofacies varies as follows (Figure 18): nonlaminated to slightly laminated foraminifera wackestones (0.69); nonlaminated siliceous and fossiliferous claystones (0.68); and highly fossiliferous moderate- to well-laminated organic-rich mudstones

(0.56). Pore microstructures of the Galembó Member shales were defined by grain size (typically of micrometric scale) and mineral composition.

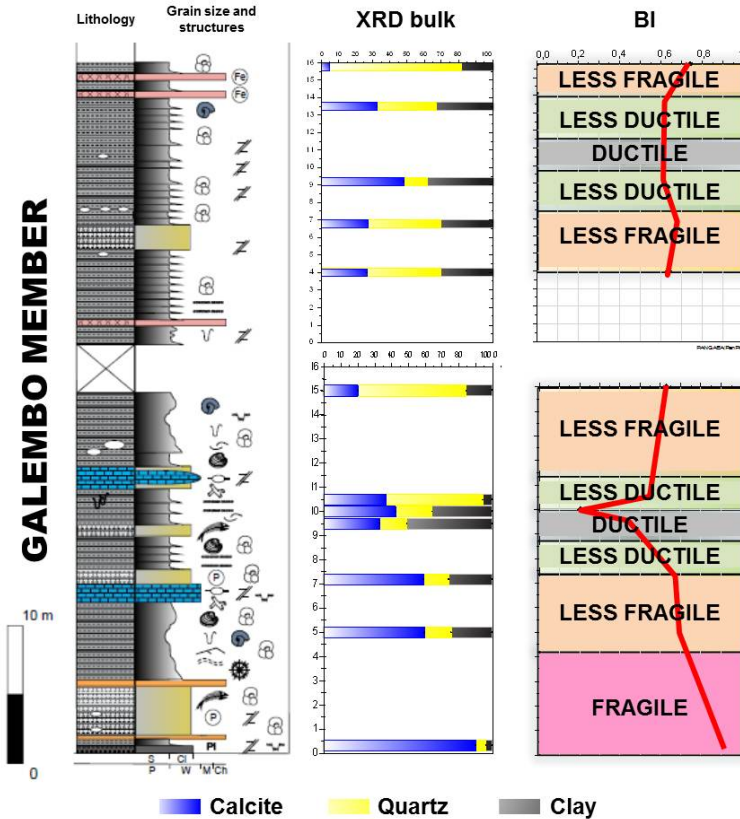


Figure 18: Brittle and ductile zones obtained with the brittleness index according to Slatt and Abousleiman [46]. Note that samples with higher content of quartz and calcite show higher brittleness, while samples with higher clay content show higher ductility.

However, the content of clay minerals is variable and often other mineral phases, such as quartz and calcite are dominant in these low permeability mudstones. A compaction process reduced the porosity of shales and aligned flakes of clay minerals in shales during and after deposition.

Shales contain significant quantities of organic matter in the form of bitumen and gas, which are formed during thermal maturation and play a very important role in their physical and chemical characteristics. Organic matter contributes to decrease density, impart anisotropy, alter wettability, introduce adsorption, and perhaps, most importantly, increase porosity [49]. Pore microstructures also affect geomechanical properties [46]. The nature of shales makes microstructural investigations by conventional scanning electron microscopy imaging of fractured surfaces is still of valuable importance. Evidently, there are methods for gathering three-dimensional images of the porosity, such as argon-ion milling and/or field emission scanning electron microscopy, which are well documented and discussed for unconventional gas shales, however, freshly broken surfaces of shales are also very helpful to estimate their 3D porosity. It is well known that microstructural features of organic-rich shales become progressively more visible and quantifiable by moving from polished to ion-milled surfaces [49], and, therefore, we are also considering to avoid mechanically polished surfaces, which can partially or totally remove the organic matter or clay minerals.

5 Conclusions

Characterizing the Galembo Member of the La Luna Formation, a primary assessment indicates a good potential for a shale gas system, where abundant organic matter content (the average TOC content is 4.5%, with a minimum of 0.6% and a maximum of 7.5%) is present, the formation has reached maturity levels and has relatively high porosity (less than 5%, and is lower in rocks with a microspar matrix and higher in rocks with a high content of fossils with a clay matrix) for hydrocarbon storage. The integration of different stratigraphic and mineralogical data for lithofacies analysis led to recognize five general lithofacies in the Aguablanca section: (1) nonlaminated to slightly laminated foraminifera wackestones, (2) highly fossiliferous moderate- to well-laminated organic-rich mudstones; (3) claystones with fossiliferous carbonate concretions with pyrite; (4) non-laminated siliceous and fossiliferous claystones; (5) volcanic ash falls. We illustrate several examples of a variety of pore types that are present in the Galembo Member of the La Luna Formation. The pores observed in the analyzed samples are enough not only to store hydrocarbon molecules

but also to promote their flow through pathways. This porosity is associated to flocculation of clays probably with the greatest potential, along with microfractures and organoporosity, to provide storage places as well as permeability pathways for migration of hydrocarbons. A combination of hand-sample observation, thin-section description, FEG ESEM and EDS analysis, are very useful for identifying and documenting the occurrence of the pore types in the investigated rocks. We conclude that grains that make up the facies of the Aguablanca section are intra-basin (foraminifera, undifferentiated bioclasts, calcareous matrix, etc.) and extra-basin (fall ash, detrital quartz, etc.). It could be estimated that the composition of these grains varies from base to top of the section and was studied with various techniques that were integrated to give consolidated information that can mark lithological changes. The data collected and analyzed helped to differentiate two units in the Aguablanca section. Changes in calcareous and clayey mineralogy have a lateral and vertical variation. The fragile and ductile zones obtained with the fragility index show that with a higher content of quartz and calcite there is a higher fragility index, while samples with a higher content of clay and organic matter are more ductile.

Acknowledgements

This work forms part of the MSc Thesis carried out by E. Casadiego at the School of Geology of the Universidad Industrial de Santander. The authors thank to the Universidad Industrial de Santander for allow the use of research facilities at the Guatiguará Technological Park: the Laboratory of Transmitted Light Microscopy of the Research Group in Basic and Applied Geology of the School of Geology, and the Laboratory of Microscopy of the Vicerrectoría de Investigación y Extensión and their professional staff for assistance with SEM data acquisition and analyses. The authors also acknowledge to the anonymous referees for their critical and insightful reading of the manuscript. We are most grateful to the above-named people and institutions for support.

References

- [1] B. E. Law and J. B. Curtis, "Introduction to unconventional petroleum systems," *AAPG Bulletin*, vol. 86, no. 11, pp. 1851–1852, 2007. <https://doi.org/10.1306/61EEDDA0-173E-11D7-8645000102C1865D> 171
- [2] M. Josh, L. Esteban, C. D. Piane, J. Sarout, D. N. Dewhurst, and M. B. Clennell, "Laboratory characterization of shale properties," *Journal of Petroleum Science and Engineering*, vol. 88-89, pp. 107–124, 2012. <https://doi.org/10.1016/j.petrol.2012.01.023> 171
- [3] R. G. Loucks, R. M. Reed, S. C. Ruppel, and U. Hammes, *Spectrum of pore types in siliceous mudstone in shale gas systems (Abstract)*. AAPG/SEG/SPE/SPWLA, 2010. 171
- [4] Q. R. Passey, K. Bohacs, W. L. Esch, R. Klimentidis, S. Sinha, and Others, "From oil-prone source rock to gas-producing shale reservoir-geologic and petrophysical characterization of unconventional shale gas reservoirs," in *International oil and gas conference and exhibition in China*. Society of Petroleum Engineers, 2010. 171, 182, 184, 189
- [5] C. H. Sondergeld, R. J. Ambrose, C. S. Rai, and J. Moncrieff, "Microstructural studies of gas shale: Society of Petroleum Engineers," in *SPE 131768 Unconventional Gas Conference, Pittsburgh (USA)*, 2010. 171, 189
- [6] D. Barrero, A. Pardo, C. A. Vargas, and J. F. Martínez, "Colombian sedimentary basins: Nomenclature, boundaries and petroleum geology, a new proposal," *Agencia Nacional de Hidrocarburos*, vol. 1, p. 92, 2007. 172, 173
- [7] L. G. Morales, D. J. Podesta, W. C. Hatfield, H. Tanner, S. H. Jones, M. H. Barker, D. J. O'Donoghue, C. E. Mohler, E. P. Dubois, C. Jacobs, and C. R. Goss, "General Geology and oil occurrences of the Middle Magdalena Valley, Colombia: South America," in *Habitat of Oil Symposium*, L. G. Weeks, Ed. AAPG, 1958, pp. 641–695. 172, 173, 174
- [8] S. Schamel, "Middle and Upper Magdalena Basins, Colombian," in *Active Margin Basins*, K. T. Biddle, Ed. AAPG, 1991, pp. 283–301. 172
- [9] J. C. Rodriguez, "Challenges and opportunities for the development of Shale resources in Colombia," Master's thesis, The University of Texas, Austin (USA), 2013. 172
- [10] J. Zumberge, "Source Rocks of the La Luna Formation (Upper Cretaceous) in the Middle Magdalena Valley, Colombia," in *Petroleum Geochemistry and Source Rock Potential of Carbonate Rocks*, J. Palacas, Ed. AAPG Special Volumes, 1984, pp. 127–133. 172, 173, 174

- [11] J. C. Ramon and L. I. Dzou, “Petroleum geochemistry of the Middle Magdalena Valley: Colombia,” *Organic Geochemistry*, vol. 30, no. 4, pp. 249–266, 1999. <https://doi.org/10.1016/j.marpetgeo.2003.11.019> 172
- [12] A. Rangel, P. Parra, and C. Niño, “The La Luna Formation: chemostratigraphy and organic facies in the Middle Magdalena Basin,” *Organic Geochemistry*, vol. 31, no. 12, pp. 1267–1284, 2000. [https://doi.org/10.1016/S01466380\(00\)00127-3](https://doi.org/10.1016/S01466380(00)00127-3) 172, 173, 174
- [13] R. C. Aguilera, V. A. Sotelo, C. A. Burgos, C. Arce, C. Gómez, J. Mojica, H. Castillo, D. Jiménez, and J. Osorno, “Organic Geochemistry Atlas of Colombia: An Exploration Tool for Mature and Frontier Basins,” *Earth Sciences Research Journal*, vol. 13, pp. 1–174, 2009. 172
- [14] E. J. Torres, “Unconventional gas shale assessment of La Luna Formation in the central and south areas of the Middle Magdalena Valley Basin, Colombia,” Master’s thesis, University of Oklahoma, Norman (USA), 2013. 172, 196
- [15] A. Young, P. H. Monaghan, and R. T. Schweisberger, “Calculation of ages of hydrocarbons in oils - Physical chemistry applied to petroleum geochemistry I,” *AAPG Bulletin*, vol. 61, no. 4, pp. 573–600, 1977. 172
- [16] S. Talukdar, O. Gallango, and A. Ruggiero, “Formaciones La Luna y Querecual: rocas madres de petróleo,” in *Memorias VI Congreso Geológico Venezolano*, A. Espejo, J. H. Ríos, N. P. D. Bellizzia, and A. S. D. Pardo, Eds. Caracas, Venezuela: Sociedad Venezolana de Geólogos, 1985, pp. 3606–3642. 172
- [17] Google, “Google Earth,” 2018. <http://earth.google.com> 173
- [18] D. A. Piamonte and L. A. Mayorga, “Caracterización de Yacimientos Tipo Shale Gas y Oil Shale en La Formación La Luna en el Flanco Oriental de la Cuenca del Valle Medio del Magdalena (VMM), Santander, Colombia,” Master’s thesis, Universidad Industrial de Santander, Bucaramanga (Colombia), 2015. 174
- [19] R. L. Folk, *Petrology of Sedimentary Rocks*. Austin: Hemphill Publishing Company, 1974. 174
- [20] R. J. Dunham, “Classification of Carbonate Rocks According to Depositional Texture,” in *Classification of Carbonate Rocks*, W. E. Hamm, Ed. AAPG Memoir, 1962, pp. 108–121. 174
- [21] R. V. Ingersoll, T. F. Bullard, R. L. Ford, J. P. Grimm, J. D. Pickle, and S. W. Sares, “The effect of grain size on detrital

- modes: A test of the Gazzi-Dickinson point-counting method,” *Journal of Sedimentary Petrology*, vol. 54, no. 1, pp. 103–116, 1984. <https://doi.org/10.1306/212F8783-2B24-11D7-8648000102C1865D> 175
- [22] R. Kretz, “Symbols for rock-forming minerals,” *American Mineralogist*, vol. 68, pp. 277–279, 1983. <https://doi.org/10.1007/978-3-540-74169-5> 175
- [23] E. Casadiego, “Caracterización de reservorios de gas shale integrando datos multiescala: Caso estudio Miembro Galembo, Sección Aguablanca, Cuenca del Valle Medio del Magdalena,” Master’s thesis, Universidad Industrial de Santander, Colombia, 2014. 175, 179, 182
- [24] R. H. Bennett, N. R. O’Brien, and M. H. Hulbert, “Determinants of clay and shale microfabric signatures: processes and mechanisms,” in *Microstructure of Fine Grained Sediments: From Mud to Shale*, R. H. Bennett, W. R. Bryant, M. H. Hulbert, W. A. Chiou, R. W. Faas, J. Kasprowicz, H. Li, T. Lomenick, N. R. O’Brien, S. Pamukcu, P. Smart, C. E. Weaver, and T. Yamamoto, Eds. New York: Springer-Verlag, 1991, pp. 5–32. 182, 187
- [25] N. R. O’Brien and R. M. Slatt, “The fabrics of shales and mudstone, an overview,” in *Proceedings of the Clay Minerals Society 27th Annual Meeting-39th Annual Clay Minerals Conference, Missouri (USA)*, 1990. 182, 183, 187
- [26] S. Creaney and Q. R. Passey, “Recurring patterns of total organic carbon and source rock quality within a sequence stratigraphic framework,” *AAPG Bulletin*, vol. 77, no. 3, pp. 386–401, 1993. <https://doi.org/10.1306/bdff8c18-1718-11d78645000102c1865d> 182
- [27] M. Skalinski and J. Kenter, “Pore Typing Workflow for Complex Carbonate Systems,” in *AAPG Annual Convention and Exhibition, Pittsburgh (USA)*, may 2013. 184
- [28] J. Schneider, P. B. Flemings, R. J. Day-Stirrat, and J. T. Germaine, “Insights into porescale controls on mudstone permeability through resedimentation experiments,” *Geology*, vol. 39, pp. 1011–1014, 2011. <https://doi.org/10.1130/G32475.1> 184
- [29] R. M. Slatt and N. R. O’Brien, “Pore types in the Barnett and Woodford gas shales: contribution to understanding gas storage and migration pathways in fine grained rocks,” *AAPG Bulletin*, vol. 95, no. 12, pp. 2017–2030, 2011. <https://doi.org/10.1306/03301110145> 184, 185, 187, 189, 191, 192, 194
- [30] S. Bernard, B. Horsfield, H. M. Schulz, R. Wirth, A. Schreiber, and N. Sherwood, “Geochemical evolution of organic-rich shales with increasing maturity: a STXM and TEM study of the Posidonia Shale (Lower Toarcian,

- northern Germany),” *Marine and Petroleum Geology*, vol. 31, pp. 70–89, 2012. <https://doi.org/10.1016/j.marpetgeo.2011.05.010> 184
- [31] G. R. Chalmers, R. M. Bustin, and I. M. Power, “Characterization of gas shale pore systems by porosimetry, pycnometry, surface area, and field emission scanning electron microscopy/transmission electron microscopy image analyses: Examples from the Barnett, Woodford, Haynesville, Marcellus, and Doig uni,” *AAPG bulletin*, vol. 96, no. 6, pp. 1099–1119, 2012. <https://doi.org/10.1306/10171111052> 184
- [32] R. M. Slatt, P. Philip, Y. Abousleiman, P. Singh, R. Perez, K. Portas, J. Marfurt, N. Madrid-Arroyo, E. O’Brien, V. Eslinger, and E. Baruch, “Pore-to-regional-scale, integrated characterization workflow for unconventional gas shales,” in *Shale reservoirs-Giant resources for the 21st century*, J. Breyer, Ed. AAPG Memoir, 2012, pp. 127–150. 184, 185, 187, 189, 192, 196
- [33] L. M. Keller, L. Holzer, R. Wepf, and P. Gasser, “3d geometry and topology of pore pathways in Opalinus clay: implications for mass transport,” *Applied Clay Science*, vol. 52, pp. 85–95, 2011. <https://doi.org/10.1016/j.clay.2011.02.003> 184
- [34] M. E. Curtis, R. J. Ambrose, C. H. Sondergeld, and C. S. Rai, “Microstructural investigation of gas shales in two and three dimensions using nanometer-scale resolution imaging,” *AAPG Bulletin*, vol. 96, no. 4, pp. 665–677, 2012. <https://doi.org/10.1016/j.jngse.2019.102907> 184
- [35] R. G. Loucks, R. M. Reed, S. C. Ruppel, and D. M. Jarvie, “Morphology, genesis, and distribution of nanometer-scale pores in siliceous mudstones of the Mississippian Barnett Shale,” *Journal of Sedimentary Research*, vol. 79, pp. 848–861, 2009. <https://doi.org/10.2110/jsr.2009.092> 184, 188
- [36] J. Klaver, G. Desbois, J. L. Urai, and R. Littke, “Bib-sem study of the pore space morphology in early mature Posidonia Shale from the Hils area, Germany,” *International Journal of Coal Geology*, vol. 103, no. 1, pp. 12–25, 2012. <https://doi.org/10.1016/j.coal.2012.06.012> 184
- [37] R. G. Loucks, R. M. Reed, S. C. Ruppel, and U. Hammes, “Spectrum of pore types and networks in mudrocks and a descriptive classification for matrix-related mudrock pores,” *AAPG Bulletin*, vol. 96, no. 6, pp. 1071–1098, 2012. <https://doi.org/10.1306/08171111061> 184, 189, 195
- [38] D. Jarvie, R. J., T. E. R. Hill, and R. M. Pollastro, “Unconventional shale-gas systems: The Mississippian Barnett Shale of north-central Texas as one model for thermogenic shale-gas assessment,” *AAPG Bulletin*, vol. 91, no. 4, pp. 475–499, 2007. <https://doi.org/10.1306/12190606068> 188, 196

- [39] H. Eltom, O. Abdullatif, M. Makkawi, and A. Abdullraziq, “Microporosity in the Upper Jurassic Arab-D carbonate reservoir, central Saudi Arabia: an outcrop analogue study,” *Journal of Petroleum Geology*, vol. 36, no. 3, pp. 281–297, 2013. <https://doi.org/10.1111/jpg.12556> 189, 192
- [40] J. F. W. Gale and J. Holder, “Natural fractures in some US. shales and their importance for gas production,” in *Petroleum Geology Conference Series*, vol. 7. Geological Society, 2010, pp. 1131–1140. 192
- [41] R. M. Slatt, “Important Geological Properties of Unconventional Resource Shales,” *Central European Journal of Geosciences*, vol. 3, no. 4, pp. 435–448, 2011. <https://doi.org/10.2478/s13533-011-0042-2> 194
- [42] S. Xian, G. Liu, Y. Chenga, L. Yang, H. Jiang, L. Chen, S. Jiang, and J. Wang, “Brittleness index prediction in shale gas reservoirs based on efficient network models,” *Journal of Natural Gas Science and Engineering*, vol. 35, pp. 673–685, 2016. <https://doi.org/10.1016/j.jngse.2016.09.009> 196
- [43] N. Lou, T. Zhao, and Y. Zhang, “Calculation Method about Brittleness Index in Qijia Oil Field,” *IOSR Journal of Engineering (IOSRJEN)*, vol. 6, no. 3, pp. 14–19, 2016. 196
- [44] F. P. Wang and J. F. W. Gale, “Screening criteria for shale-gas systems,” *Gulf Coast Association of Geological Societies Transactions*, vol. 59, pp. 779–793, 2009. 196
- [45] Z. Guo, X.-Y. Li, C. Liu, X. Feng, and A. Y. Shen, “Shale rock physics model for analysis of brittleness index, mineralogy, and porosity in the Barnett Shale,” *Journal of Geophysics and Engineering*, vol. 10, no. 2, p. 25006, 2013. <https://doi.org/10.1088/1742-2132/10/2/025006> 196
- [46] R. M. Slatt and Y. Abousleiman, “Merging sequence stratigraphy and geomechanics for unconventional gas shales,” in *The Leading Edge, Special Section: Shales*, 2011, pp. 274–282. <https://doi.org/10.1190/1.3567258> 196, 197, 198
- [47] T. Dong, N. B. Harris, K. Ayranci, C. E. Twemlow, and B. R. Nassichuk, “Porosity characteristics of the Devonian Horn River shale, Canada: Insights from lithofacies classification and shale composition,” *International Journal of Coal Geology*, vol. 141, pp. 74–90, 2015. <https://doi.org/10.1016/j.coal.2015.03.001> 196
- [48] A. Gómez, “Integrated geological characterization and distribution of the Salada member, La Luna Formation in the central area of The Middle Magdalena Basin, Colombia,” Master’s thesis, University of Oklahoma (USA), 2014. 196

- [49] A. R. Butcher and H. J. Lemmens, “Advanced SEM Technology Clarifies Nanoscale Properties Of Gas Accumulations In Shales,” *The American Oil & Gas Reporter*, 2011. <https://www.aogr.com/magazine/cover-story/advanced-semtechnology-clarifies-nanoscale-properties-of-gas-accumulations> 198